New Abrasive Coatings: Abraded Volume Measurements in Ceramic Ball Production

Journal of
Manufacturing and Materials Processing

MDPI

Article

New Abrasive Coatings: Abraded Volume Measurements in Ceramic Ball Production

Irene Pessolano Filos [1], Raffaella Sesana [1,*], Massimiliano Di Biase [2] and Rocco Lupoi [3]

[1] DIMEAS, Politecnico di Torino, Corso Duca degli Abruzzi 24, 10129 Torino, Italy; irene.pessolano@polito.it
[2] Central Lab—Product Development, Tsubaki Nakashima, Corso Torino, 378, 10064 Pinerolo (TO), Italy; massimiliano.dibiase@studenti.polito.it
[3] Department of Mechanical, Manufacturing & Biomedical Engineering, Trinity College Dublin, The University of Dublin, Parsons Building, Dublin 2, Ireland; lupoir@tcd.ie
* Correspondence: raffaella.sesana@polito.it; Tel.: +39-011-0906-907

Abstract: Technological progress in hybrid bearings developed high wear and abrasion resistant materials for rolling elements. The manufacturing process of bearing balls presents new challenges, as nowadays, it requires time-consuming and costly processes. In this frame, the bearing manufacturing industry is demanding improvements in materials, geometry, and processes. This work aims to investigate new abrasive coatings for grinding wheels for Si_3N_4 ball manufacturing. Tribological pin on disk tests are performed on samples of grinding materials (disk) versus a Si_3N_4 ball (pin). Two samples of specimens coated with an electrodeposited diamond and diamond-reinforced metal matrix composite are examined to measure the abrasion rate and the wear resistance of Silicon Nitride Si_3N_4 balls, considering the influence of sliding speed and the effect of coating deposition on diamond particle density and granulometry. The measurements estimated the specific wear coefficient k, the height wear surface h, and the wear rate u of the Si_3N_4 balls. The results pointed out that by increasing the sliding speed, the abraded volume increases for both the coatings. The parameters affecting the abrasion effectiveness of both the coatings are the surface roughness, the abrasive particle dimension, and the sliding speed.

Keywords: abrasive coating; ceramic rolling bodies; abrasion

Citation: Pessolano Filos, I.; Sesana, R.; Di Biase, M.; Lupoi, R. New Abrasive Coatings: Abraded Volume Measurements in Ceramic Ball Production. *J. Manuf. Mater. Process.* **2021**, *5*, 81. https://doi.org/10.3390/jmmp5030081

Academic Editors: Swee Hock Yeo, Arun Prasanth Nagalingam and Carsten Heinzel

Received: 20 May 2021
Accepted: 22 July 2021
Published: 27 July 2021

1. Introduction

Technological progress has led to the development of hybrid bearings that entail the use of ceramic rolling elements characterized by a high bearing stiffness, low weight, non-negligible self-lubricating properties, high corrosion resistance, and electric insulation [1–4]. Because of their peculiar physical, thermal, and mechanical properties, these bearings have been considered for several applications, including those related to the production of electric motors, medical equipment, machine tool spindles, and turbine generators [5–7]. In [8], a wide review of applications of hybrid bearings is presented.

Since ceramic bearings are highly resistant to wear and abrasion, their manufacturing, which is traditionally based on the use of diamond paste and grinding wheels, which operate by abrasion, presents several challenges. Wheels are generally made of Cast Iron, while the abrasive coating is composed of electrodeposited Diamond particles. The manufacturing process is time-consuming and complex, as it involves the removal of material both from the ball surface and from the grinding wheel. This action generates heat, and it evolves in time as a function of both the ball surface parameters (roughness) and the grinding wheel surface condition (abrasive particles removal). Given the complexity of these phenomena, the bearing manufacturing industry is demanding improvements in materials, geometry, and process parameters calibration.

With respect to the coating of grinding wheels, many technological solutions adopted by the industry stem from experience cumulated in the use of Diamond paste or Diamond

based coatings in machinery tools for grinding [9], lapping [10], and polishing operations [11,12]. The literature indicates that there are many different methods available to cover a substrate with a hard-protective layer, [13] provide a useful review in which the main coating techniques are listed and compared to one another, with the identification of the main advantages and disadvantages.

The most widely used techniques to produce thin coatings are physical vapor deposition (PVD) [14], chemical vapor deposition (CVD), electrodeposition and cold spraying. PVD and CVD fall within the category of vapor-phase plasma-based deposition methods and allow high-quality coatings with no limitation on the coating or substrate material. The layers obtained usually have a thickness ranging from 2 to 10 μm and are particularly suited to improve sliding wear and low-stress abrasive wear. For what concerns electrodeposition, a deep review is presented in [15]. The principles of the electrodeposition process are based on the electrochemical phenomena associated with the reduction or deposition of electroactive species on the cathode surface. The empirical factors affecting the electrodeposition process are many; however, it can be precisely controlled [16]. In recent years, a new deposition technique is gaining momentum: Cold-Spray deposition. More details about the surface coating technique can be found in [17]. Gas dynamic cold spraying or Cold Spraying is a coating deposition method in which solid powders (1 to 50 μm in diameter) are accelerated in a supersonic gas jet to velocities up to 1200 m/s. During the impact with the substrate, particles undergo plastic deformation and adhere to the surface. To achieve a uniform thickness, the spraying nozzle is scanned along the substrate. Metals, polymers, ceramics, composite materials, and nanocrystalline powders can be deposited using cold spraying. The kinetic energy of the particles, supplied by the expansion of the gas, is converted to plastic deformation energy during bonding. Unlike thermal spraying techniques, e.g., plasma spraying, arc spraying, flame spraying, or high-velocity Oxygen fuel (HVOF), the powders are not melted during the spraying process [18].

In industrial applications for surface processing and finishing manufacturing processes of components, coatings are applied to abrasive wheels with the above-mentioned techniques. The use of metal matrix diamond composite for abrasive application of wear-resistant material was already investigated in [19], and since then, following the development of coating techniques, the implementation of diamond metal composites had spread in machining applications. Recently, diamond-reinforced metal matrix composites (DMMC) have been investigated for alternative abrasive coatings [18] and tools [20]. Numerous investigations have focused on the tribological wear and behavior of diamond reinforced composites coating, for example, in [21], where microstructure and the distribution of diamond and tungsten carbide are investigated, and in [14] and in [15], where the influence of the processing parameters on wear of coating of respectively PVD and electrodepositionis investigated, and the different techniques used to depose it [22]. Moreover, there are several aspects that affect the reinforced composites coatings, such as diamond size [23], coating thickness [24], or thermal conductivity [25,26]. DMMC durability in aggressive abrasive conditions has been studied [20]. This technique also applies well to multilayer coatings [27].

For what concerns bearing balls manufacturing when abrasion is required, the traditional abrasive approach is required, even if other approaches are presented in the literature as in [28] where an apparatus based on a completely different approach, that is, magnetic floating, is presented for polishing of Si_3N_4 balls.

Investigating the abrasive process of bearing balls involves quantifying the abrasion properties of the different coating and coating processes, that is, on one side investigating the wear resistance and adhesion properties of the coating and on the other side investigating the capability of the coating to abrade the balls. The first topic is widely investigated in the literature, and a dedicated Standard is available; for example, the two and three-body abrasion testers are described in [29,30] to test the adhesion and wear resistance of coatings. For example, in [21], wear tests are performed by means of a two-body abrasion tester. The wear rate is measured from the weight loss and expressed as the volume loss per

unit distance run in wear testing. In [20], the volume loss rate and the mass loss rate, the particle distribution, and homogeneities are investigated for metal matrix composites (MMC) obtained with diamond particles charges for different diamond grits deposited on a stainless-steel substrate. Abrasion tests were performed according to the ASTM G65 Standard, which is a dry sand/rubber wheel apparatus. The results confirmed the beneficial effect of the nickel coating on the diamond in producing an improved abrasion resistance. In [31], a large investigation on the grinding performance of electrodeposited diamond wheels for hard metals against ceramic is reported. Eighteen kinds of synthetic diamond abrasive grains are compared. The peripheral speed of a wheel at tests was (1000 m/min) and thrust constant pressure of grinding was (490 kPa). Grinding time, stock removal, tangential and normal grinding force were measured. In particular, the parameters grinding work and cumulative grinding work are defined as the sum of the integrals of the grinding normal and tangential forces over grinding length for a given path and for all the paths, respectively. The removed volume (stock removal) is in the paper plotted vs. the grinding work. No standard procedure or equipment is described and applied in this work. In [23], pin on disk tests are run with a 4 mm Si_3N_4 ceramic ball (pin), with a 550 g (5.4 N) load, 500 rpm, and 5 mm diameter wear track. In this paper, an analysis of the effects of the diamond size and Ni matrix on the deposition characteristics are presented. The friction coefficient (COF) of some tests is reported, but no other tribological parameters are mentioned. In [32], both pin on disk and wear tests in dry conditions are performed but on specimens with coatings obtained with cermet powders. In this paper, the COF between the different coatings and the pin is investigated, and the wear track is reconstructed after the pin on disk tests by means of 3D microscopy, allowing measurement of the coating removed volume and wear track diameter. Roughness measurements of the substrate were performed to integrate the investigation on adhesion coating behavior. A similar experimental approach is reported in [21], where the scar trace is investigated to quantify the removed volume and the abrasion performance of different coatings. The friction coefficient and the wear rate are simultaneously investigated by means of two-body abrasion tests. In the quantitative and qualitative investigation of wear and friction problems, a specific thought can be given to a piece of new equipment able to reconstruct in real-time the wear scar thanks to a pin-on-disc tribometer equipped with a Digital Holographic Microscope (DHM) [33].

For the second topic, which is investigating the capability of the coating to abrade the balls, the problem of wear testing and wear volume loss measurement are faced in international standards as per [34–36]. In these documents, the testing equipment, procedure, and the abraded volume measurements are described. Pin on disk testing is widely used both for investigating tribological and wear behaviors of mating materials. Special dedicated equipment is used to test in critical conditions like cryogenic testing, as described in [37]. The same test can cover two different problems and different approaches. If the focus is on the force required to rotate the disk pushed by the pin, then friction parameters are obtained; however, if the focus is volume abraded by friction phenomena, then wear parameters are obtained. In [38], two testing procedures for the diagnosis of commercial pin-on-disc tribometers are described and proposed as reference procedures. In the above-mentioned Standards, the abraded volume is quantified by means of profile, microscope and dimensional measurements of the samples before and after testing. For example, in [6], pin on disk tests results are reported and related to the friction of alumina balls against diamond ceramic coating for prosthetic application. In this research, the wear volume and wear rate are measured according to [36], and the worn ball radius is measured by an optical microscope.

The purpose of this paper is to assess the effects of two different diamond coatings (electrodeposited diamond paste and cold sprayed DMMC) on the wear resistance and final surface characteristics of Silicon Nitride (Si_3N_4) bearings. In such a context, laboratory tests were carried out by means of the pin-on-disk approach while considering the impact on test results of several operational variables (e.g., rotating speed and test geometry).

Results were interpreted by referring to meaningful wear and tribological parameters and by considering the different composition and surface morphology of the two coatings. As illustrated in the final section of the paper, it is envisioned that obtained results can be of practical use for the optimization of the manufacturing process of ceramic ball bearings.

2. Materials and Methods

The experimental investigation described in this paper involved the use of Si_3N_4 ceramic bearing balls (nominal diameter 6 mm) and two different diamond coatings employed in pin-on-disk tests: a diamond-reinforced metal matrix composite cold-sprayed on an Aluminium substrate (indicated as DMMC), and a synthetic diamond coating with a maximum particle size of 30 μm electrodeposited on a Cast Iron substrate (indicated as D30). Sample preparation was carried out as described in Section 2.1 in collaboration between the Politecnico di Torino (Torino, Italy), the Tsubaki Nakashima Internal Application Laboratory (Pinerolo, Italy), and the STAM Research Center of the Department of Mechanical, Manufacturing and Biomedical Engineering at Trinity College Dublin (Dublin, Ireland). The experimental campaign, based on the use of the tribometer equipment described in Section 2.2, was carried out in the Department of Mechanical and Aerospace Engineering Laboratory (DIMEAS) of the Politecnico di Torino (Torino, Italy).

2.1. Test samples

A total of three coated disks were prepared and subsequently used for testing. By following the procedure reported in [18], two disks (DMMC Specimen 1 and DMMC Specimen 2) were coated with DMMC (Figure 1a) by using a feedstock material constituted by copper and diamond in equal volume ratio. The copper powder was provided by Safina, while the diamond powder was supplied by Element Six. The single disk coated with D30 (Figure 1b) was prepared by LITD by means of CVD electrodeposition according to the standard method established by [13].

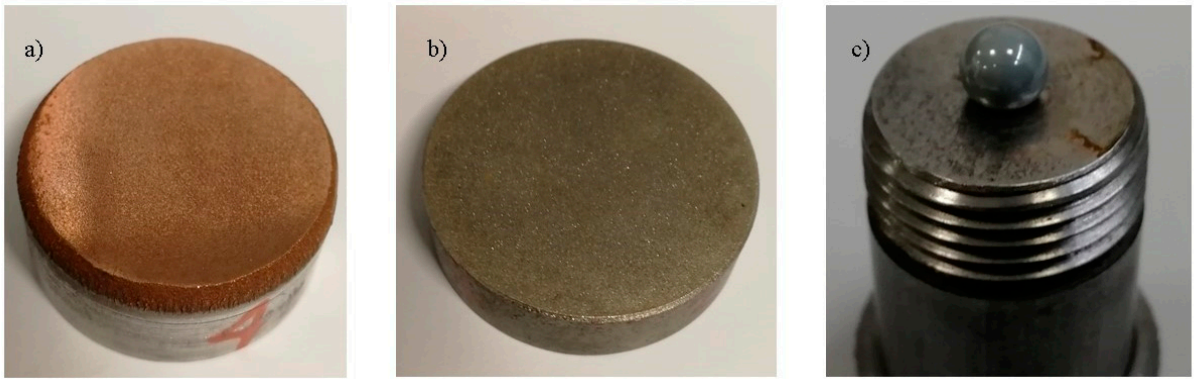

Figure 1. Samples for testing: (**a**) DMMC, (**b**) D30, and (**c**) Si_3N_4 ball.

The set of six nominally identical Si_3N_4 bearing balls employed for the investigation (Figure 1c) were retrieved from the production line of Tsubaki Nakashima. Their quality and uniformity were preliminarily assessed by visual inspection with the purpose of avoiding elements characterized by surface imperfections or defects.

Mechanical properties of the materials constituting the substrate disks (Aluminium alloy and Grey Cast Iron) and Si_3N_4 bearing balls are reported in Table 1 in terms of their average Young Modulus (E_c) and Poisson ratio (ν_c) as recorded from three independent measurements. Table 1 also contains information on the geometrical dimension of the samples (R_d, radius of the disk; R_b, radius of the balls) (mm) and on the thickness of the coatings (d_c) (μm). Coated disks were subjected to preliminary evaluation by means of a SEM, the outcomes of which are displayed in Figure 2 (front view) and Figure 3 (cross-section). Subsequent image analysis showed that in the case of the DMMC, the

employed deposition process led to a partial crushing of diamond particles, with their final dimensions being comprised in the 50–75 μm range. By comparison, the D30 coating was found to be slightly coarser, with particle dimensions comprised between 50 μm and 120 μm. The quantitative investigation on diamond particles dimension and distribution was obtained by means of image processing with ImageJ software. In Table 2, the results are reported.

Table 1. Sample dimensions and material physical properties of substrates and balls.

Material	Quantity	R_d, R_b (mm)	E_c (Gpa)	ν_c	d_c (mm)
DMMC Coating	2	15	526	0.28	3
D30 Coating	1	20	1000	0.20	0.1
Si_3N_4 Sphere	6	3	310	0.27	-

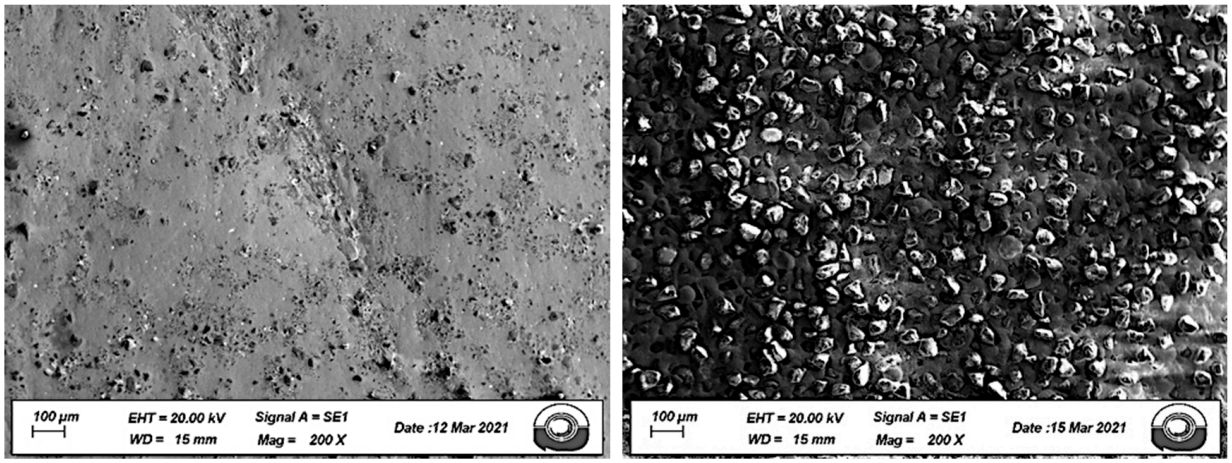

Figure 2. Microscopical front view of diamond distribution in DMMC (**left**) and D30 (**right**) coatings.

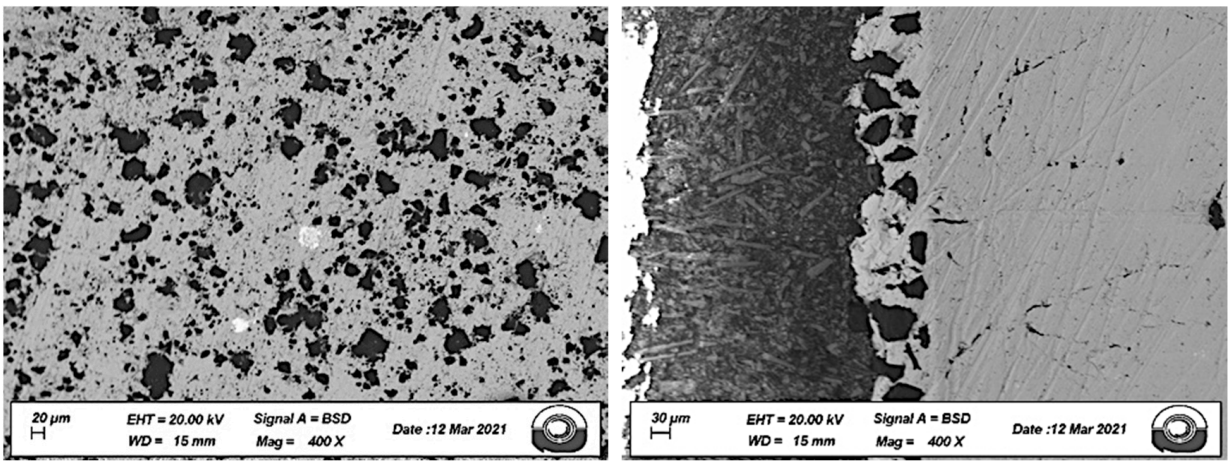

Figure 3. Microscopical section view of diamond distribution in DMMC (**left**) and D30 (**right**) coatings.

Table 2. Diamond particles dimension distribution on coated disks.

	Average Area (mm^2)	Average Diameter (mm)	Maximum Diameter (mm)	Minimum Diameter (mm)	Diameter Std. Dev
DMMC (sp. 1)	25.4	2.8	22.4	0.6	2.2
DMMC (sp. 2)	58.1	4.3	50.8	0.6	3.7
D30	1453.8	2.5	3.72	110	20.3

2.2. Test Methods

Abrasion and friction measurements were carried out in the pin-on-disk configuration by making use of the disks and bearing balls prepared as outlined in Section 2.1. Tests were performed by means of an Anton Paar TRB tribometer, the technical specifications of which are given in Table 3. The functional scheme of the equipment that is compliant with the ASTM G99 and ASTM G133 standards [34,35] is shown in Figure 4.

Table 3. Tribometer technical specifications.

Material	Quantity
Normal load (dead weight/s)	Up to 60 N
Friction force	Up to 10 N, optional 20 N
Rotation speed (Pin on Disk)	0.3–500 rpm, optional 1500 rpm
Linear speed	100 mm/s
Linear stroke	60 mm
Sample diameter	up to Ø 60 mm
Weight	0.25 N, 0.5 N, 1 N, 2 N, 5 N, 10 N, 20 N, 30 N, 60 N
Mass tolerance	±1%

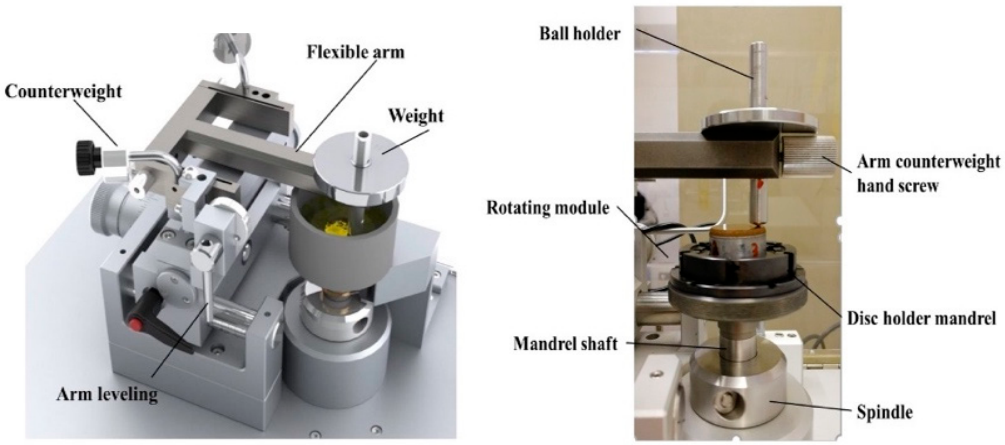

Figure 4. Functional scheme of the Anton Paar pin-on-disk tribometer and rotating module.

The first phase of the investigation was dedicated to the identification of the optimal setup parameters [39]. Given the operational characteristics of the available equipment, it was deemed necessary to explore the possibility of making use of lighter loads and lower speeds than those proposed by the original ILS (part of the actual release of the ASTM G99 standard). As a result of this preliminary work, it was concluded that for each combination of bearing ball (pin) and coated substrate (plate), two wear measurements were to be performed by imposing the pin-plate contact at 7 mm and 11 mm from the disk center and by adopting different values of the relative rotating speed (comprised between 20 rpm and 40 rpm). Normal load and sliding distance were fixed at 1 N and 150 m, respectively. Testing conditions adopted for the performed tests are synthesized in Table 4. These conditions are different from those adopted in other investigations reported in the literature. As an example, in [39–45], the normal force ranged between 10 and 20 N, the rotational speed was comprised between 200 rpm and 400 rpm, and the sliding distance varied in the 180–380 m interval. In [46], tests entailed the application of a 5 N normal load with an imposed sliding distance of 150 m.

Table 4. Test conditions.

Test Number	Coating Type	R_t (mm)	F_N (N)	n (rpm)	Local Linear Speed (mm/s)	L (m)
Test 1	DMMC (Specimen 1)	7	1	40	29.3	150
Test 2	DMMC (Specimen 1)	11	1	20	23.0	150
Test 3	DMMC (Specimen 2)	7	1	20	14.7	150
Test 4	DMMC (Specimen 2)	11	1	30	34.5	150
Test 5	D30	7	1	20	14.7	150
Test 6	D30	11	1	30	34.5	150

2.3. Data Processing

For each pin-on-disk test, wear of the contact bodies was calculated by measuring appropriate linear dimensions: length or shape change of the pin and depth or shape change of the disk track. Subsequently, wear linear measures (in mm) were converted to wear volume (in mm^3) through appropriate geometric relations reported in ASTM G99-95a [34] and ISO 18535:2016 [47] Standards.

According to ASTM G99-95a, assuming that the pin has an initial spherical surface of radius R_b and the disk is initially flat, the height from wear surface h (mm) can be calculated by means of the following expression, in which it is hypothesized that only one of the two components wears significantly [34]:

$$h = R_b - \sqrt{\left({R_b}^2 - \frac{d^2}{4}\right)} \quad (1)$$

where d is the scar diameter (mm) (Figure 5, above).

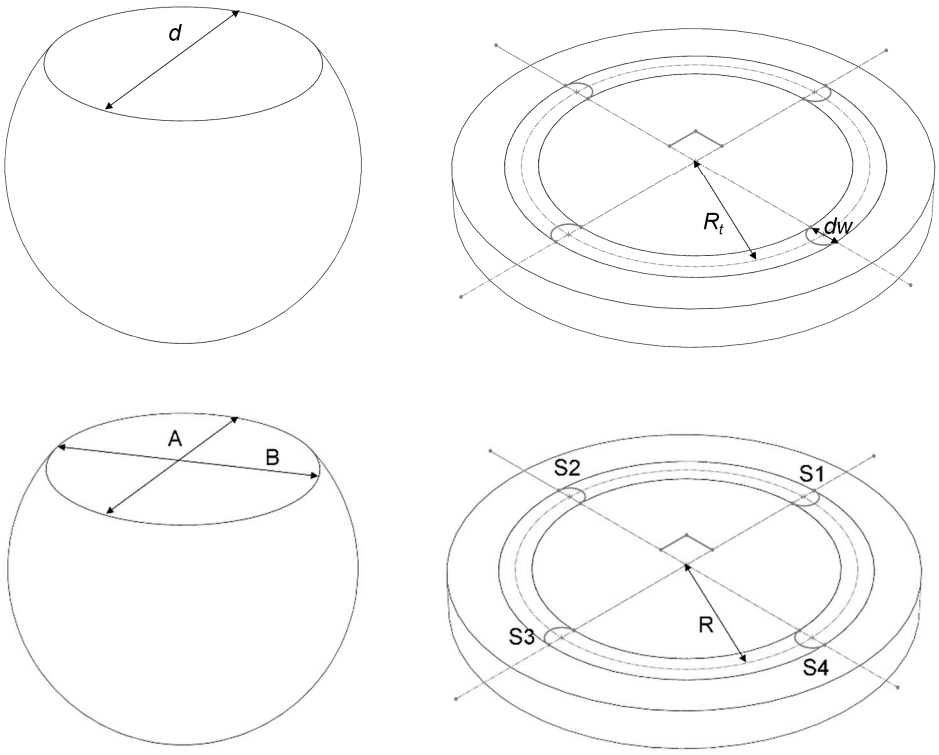

Figure 5. Wear parameter definition according to G99-95a (**above**) and according to ISO 18535 (**below**).

In the case that the ball is wearing, then the volume ball loss V_{bASTM} according to [34] is calculated as:

$$V_{bASTM} = \frac{\pi \cdot h}{6}\left[\frac{3 \cdot d^2}{4} + h^2\right] \quad (2)$$

Assuming that ball wear is negligible with respect to disk wear, then the disk volume loss V_{dASTM} can be calculated as:

$$V_{dASTM} = 2 \cdot \pi \cdot R_t \cdot \left[{R_b}^2 \cdot \arcsin\left(\frac{d}{2 \cdot R_b}\right) - \frac{d}{4}\sqrt{4{R_b}^2 - dw^2}\right] \quad (3)$$

where R_t is the track radius and dw is the width of the wear track (as in the case of [32]).

The volume losses V_b and V_d in cubic millimeters can also be calculated according to the International Standard ISO 18535:2016 [47]. According to the Standard, after the pin on disk test, it is observed that both the surfaces undergo volume losses during the test. It is then assumed that the pin presents a flat surface, and a roughly circular scar can be observed on the disk. The minimum diameter A and the perpendicular one B are measured, and the cross-sectional areas of the wear track are estimated at four positions (S1–S4) at intervals of 90° (Figure 5, below).

The wear volume V_{bISO} and the specific wear rate W_s of the balls are then calculated:

$$V_{bISO} = \frac{\pi \cdot A^3 \cdot B}{32 \cdot D} \quad (4)$$

$$W_{sb} = \frac{V_b}{F_N \cdot L} \quad (5)$$

where D is the diameter of the ball specimen (mm), F_N is the applied load (normal force) (N), and L is the sliding distance (mm). For what concerns the disk:

$$V_{dISO} = \frac{\pi \cdot R_t \cdot (S1 + S2 + S3 + S4)}{2} \quad (6)$$

$$W_{sd} = \frac{V_d}{F_N \cdot L} \quad (7)$$

where R_t is the radius of wear track (mm), and $S1$ to $S4$ represent cross-sectional areas at four places on the wear track circle (mm^2). This approach is, for example, adopted in [16]. In this research, a further parameter is defined, the percent volume loss difference Δ_{volume}, that is, the percent difference between the volumes calculated according to the two Standards:

$$\Delta_{volume} = \left|\frac{V_{b\ ISO}}{V_{b\ ASTM}} - 1\right| \quad (8)$$

In [48], another approach is proposed to quantify the wear rate in coating obtained by spraying processes. The mass loss ratio is defined as the ratio between the difference of the mass before and after the run-in wear period and the mass before the test. The mass loss is measured during the test too. On the other hand, the advantage of using linear wear measures compared to mass loss was that a more precise evaluation could be obtained since mass loss is often too small for a reliable measurement.

A further parameter quantifying wear is introduced by the Archard equations [35,36]. This approach is adopted to model the friction phenomena for the purpose of determining the wear coefficient k (adimensional) and the wear rate u (μm/h) [49–53]. Once the volume of the wear products V_b (mm^3), the sliding length L (mm), the normal force between the surfaces F_N (N), and the surface hardness HV (MPa) of the softer adherent are known, the wear coefficient k is defined as [54,55]:

$$k = \frac{V_b \cdot HV}{L \cdot F_N} \quad (9)$$

The coefficient of friction varies between an assigned pair of materials depending on load, speed, and temperature. Therefore, the coefficient of friction is measured experimentally, using the tribometer, under conditions as close as possible to the actual operating conditions. The wear equation can also be expressed as wear rate:

$$u = \frac{\delta}{t} = \frac{k \cdot P \cdot v}{HV} \quad (10)$$

where δ is the thickness of the worn layer (mm), t is time (s), HV is the hardness of the softer material (MPa), P is the interface pressure (MPa), k is the wear coefficient, and v is the sliding speed (mm/s). In the present research, the parameter u was calculated as d/t. In fact, the interface pressure cannot be calculated with a reliable formula as the contact does not occur between uniform surfaces. The last parameter used for analyzing the behavior of the two coatings is the coefficient of friction, COF, defined as the ratio between the friction resisting force and the normal force F_N applied during tribological tests. In the present research, the parameter is an output of the tribometer equipment.

2.4. Evaluation of Surface Roughness and Profile

As a supplement to wear and friction measurements, before and after the tests carried out with the tribometer, the surface roughness of pins (balls) and disks (plates) was assessed according to [29], with the consequent analysis of the recorded profiles. The Roughness Tester Mitutoyo S-3000 was employed for measuring and evaluating micro-irregularities of the surfaces. Cut off was set to 0.08 mm, measuring length was 0.4 mm, and a Gaussian filter was applied. In the case of the disk surfaces, accurate measurements were obtained by performing measurements along the X and Y axis (Figure 6) by means of a Coordinate Measuring Machine EXAGON Tigo SF (measured volume in mm is 500 × 580 × 500 in X/Y/Z directions) with an accuracy of 2.2 + 1/300 (l (mm) measured length) and a profilometer model PGS 2000. The manufacturer's technical specifications of the instrument roughness tester and profilometer are presented in Tables 5 and 6, respectively.

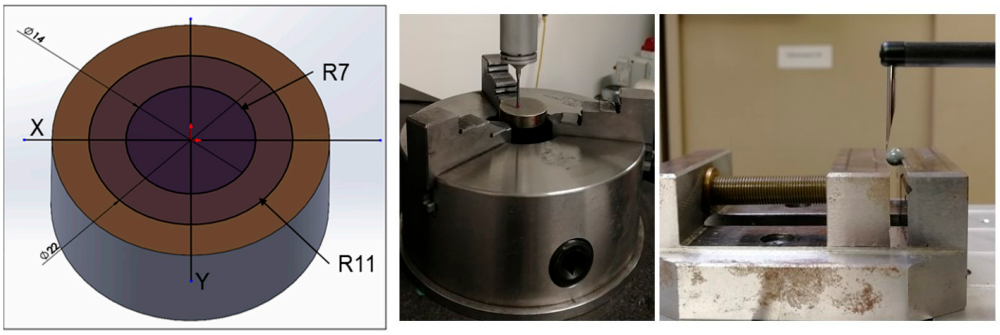

Figure 6. Surface roughness and profile study.

Table 5. Roughness tester technical specifications.

Measuring range	100 × 300 mm (X/Z)
Detector measuring force	0.75 mN
Drive speed	X: 0 ÷ 80 mm/s; Z: 0 ÷ 40 mm/s
Cut-off	800 µm, 80 µm or 8 µm

Table 6. Profilometer technical specifications.

Measurement range in X	220 mm
Measurement range in Z	50 mm
Resolution on the X axis	0.5 µm
Resolution on the Z axis	0.1 µm
Positioning speed	0–10 mm/s
Measurement speed	0.2–0.5–1–2 mm/s
Measurement tip	Tip radius 20 µm and front roundness
Software:	Profile Studio

3. Results and Discussion

Processed results of all tests were analyzed to assess the different abrasive behavior of the two considered coatings (DMMC and D30) employed to produce ceramic ball bearings. Table 7 displays the results derived from surface roughness measurements carried out on bearing balls before and after pin-on-disk tests. For ease of interpretation, the results obtained after pin-on-disk testing are also reported graphically in Figure 7.

Table 7. Surface roughness values of balls before and after testing.

		R_a (µm)	R_q (µm)	R_{pmax} (µm)	R_{vmax} (µm)	R_{zmax} (µm)
Si_3N_4 ball Test 1	Before test	0.0067	0.0096	0.0189	0.0796	0.0922
	After test	1.7312	2.0680	4.7614	4.1509	8.9271
Si_3N_4 ball Test 2	Before test	0.0069	0.0100	0.0185	0.0786	0.0892
	After test	1.8992	2.0313	2.7933	3.6621	6.4508
Si_3N_4 ball Test 3	Before test	0.0071	0.0082	0.0169	0.0801	0.0905
	After test	1.9415	2.3245	5.2471	1.5729	6.8116
Si_3N_4 ball Test 4	Before test	0.0059	0.0089	0.0201	0.0813	0.0958
	After test	1.6638	2.3526	6.3644	1.1390	7.5013
Si_3N_4 ball Test 5	Before test	0.0068	0.0091	0.0193	0.0904	0.0976
	After test	2.1775	3.3038	9.2970	1.1361	10.4239
Si_3N_4 ball Test 6	Before test	0.0091	0.0121	0.0204	0.0853	0.0799
	After test	2.9861	3.8180	11.6801	1.5413	13.2281

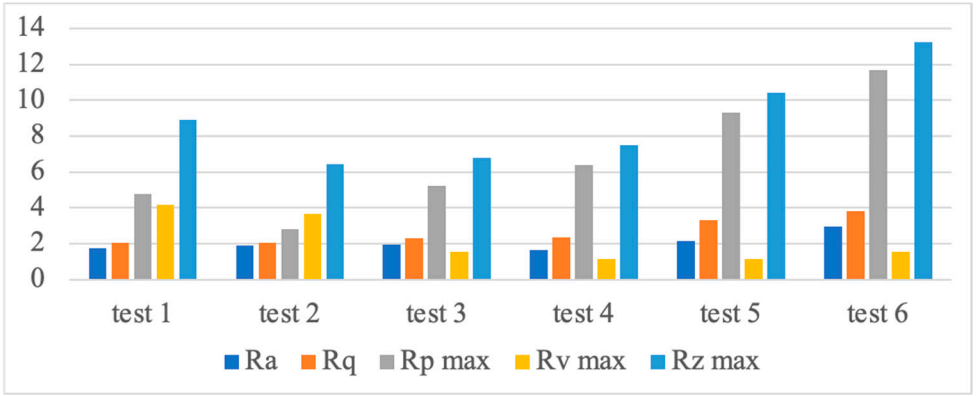

Figure 7. Surface roughness of balls after testing.

Surface roughness measurements were performed on coated disks only before pin-on-disk testing since roughness variations occurred exclusively in the wear tracks because of Si_3N_4 debris deposition. Roughness data recorded before pin-on-disk tests are listed in Table 8. Roughness parameters obtained for the disk coated with D30 are comparable to those reported in the literature [12] for polishing disks used in an industry setting to produce Si_3N_4 bearing balls. Furthermore, the data displayed in Figure 7 indicate that

in most cases (except for R_{vmax}), the roughness parameters of bearing balls subjected to abrasion with the D30 coated plate are higher than those of the balls processed in contact with DMMC. Such an outcome is consistent with the coarser surface morphology of the D30 coating, which leads to the creation of a rougher final surface.

Table 8. Surface roughness values of disks before testing.

		R_a (µm)	R_q (µm)	R_{pmax} (µm)	R_{vmax} (µm)	R_{zmax} (µm)
Test 1 and 2	Before test	0.0708	0.0851	0.2393	0.3341	0.5735
Test 3 and 4	Before test	0.0754	0.0991	0.2958	0.6530	0.8179
Test 5 and 6	Before test	3.6200	4.2186	5.2052	9.1345	14.1862

For each pin-on-disk test, the wear of the bodies in contact was calculated using both methods described in Section 2.2, thereby obtaining the results listed in Table 9 and in Table 10 for tests carried out at a distance of 7 mm and 11 mm from the disk center, respectively. Volume losses are also represented in graphical form in Figure 8.

Table 9. Results for tests carried out at R_t = 7 mm.

	$V_{b\ ASTM}$ (mm^3)	$V_{b\ ISO}$ (mm^3)	Δ_{volume}	h (mm)	W_{bs} (mm^3/(N × m))	$V_{d\ ISO}$ (mm^3)
Test 1	4.39×10^{-4}	4.30×10^{-4}	1.92%	6.83×10^{-3}	3.05×10^{-6}	3.26×10^{-2} *
Test 3	2.05×10^{-3}	2.01×10^{-3}	1.87%	1.48×10^{-2}	1.37×10^{-5}	3.89×10^{-2} *
Test 5	5.48×10^{-2}	5.08×10^{-2}	7.81%	7.66×10^{-2}	3.65×10^{-4}	7.96 *

* The positive value is due to the deposition of debris.

Table 10. Results for tests carried out at R_t = 11 mm.

	$V_{b\ ASTM}$ (mm^3)	$V_{b\ ISO}$ (mm^3)	Δ_{volume}	h (mm)	W_{bs} (mm^3/(N×m))	$V_{d\ ISO}$ (mm^3)
Test 2	1.63×10^{-3}	1.52×10^{-3}	6.76%	1.31×10^{-2}	1.08×10^{-5}	6.53×10^{-2} *
Test 4	5.36×10^{-3}	5.14×10^{-3}	4.26%	2.39×10^{-2}	3.57×10^{-5}	6.38×10^{-2} *
Test 6	1.08×10^{-1}	1.02×10^{-1}	6.46%	1.08×10^{-1}	7.23×10^{-4}	1.68 *

* The positive value is due to the deposition of debris.

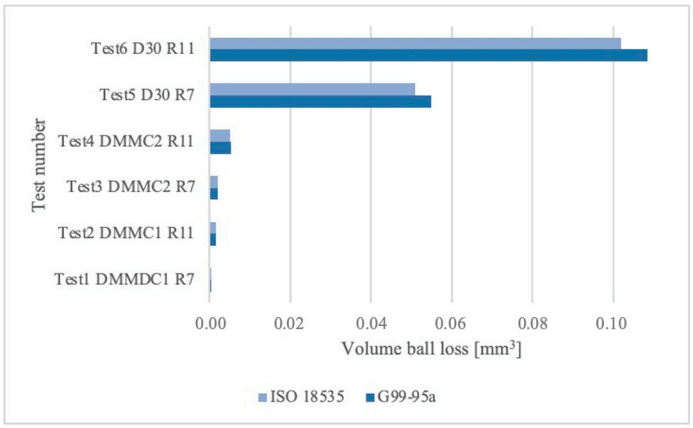

Figure 8. Comparison for ball volume loss calculation methods.

As expected, values of the sphere volume loss V_b calculated with both standards (G99 and ISO18535) were very similar. However, values of the disk volume loss V_{dISO} calculated according to ISO 18535 were found to be positive, thereby indicating a disk volume increment rather than a decrement [33,56,57]. Such an outcome can be explained by referring to the significant roughness of the disks and the deposition of debris in the surface irregularities, with the resulting conclusion that the formula proposed for the calculation of V_d may not be reliable for disks in this kind of experiment where the abraded part is

the ball (pin). This result is confirmed by profile measurements and by visual and optical microscope observation of wear track on disks (Figure 9). The measurements obtained by means of the profilometer along a diameter (Y direction) are reported in Figure 10 as an example before and after testing. It is evident that the wear of the disks can be neglected if compared with the wear of balls.

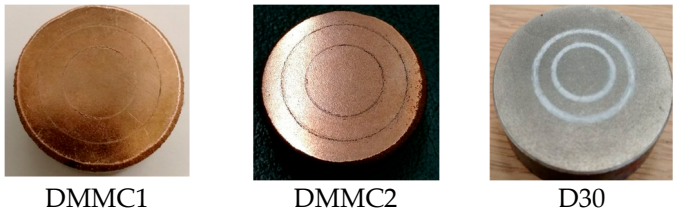

Figure 9. Wear scars on disks after test.

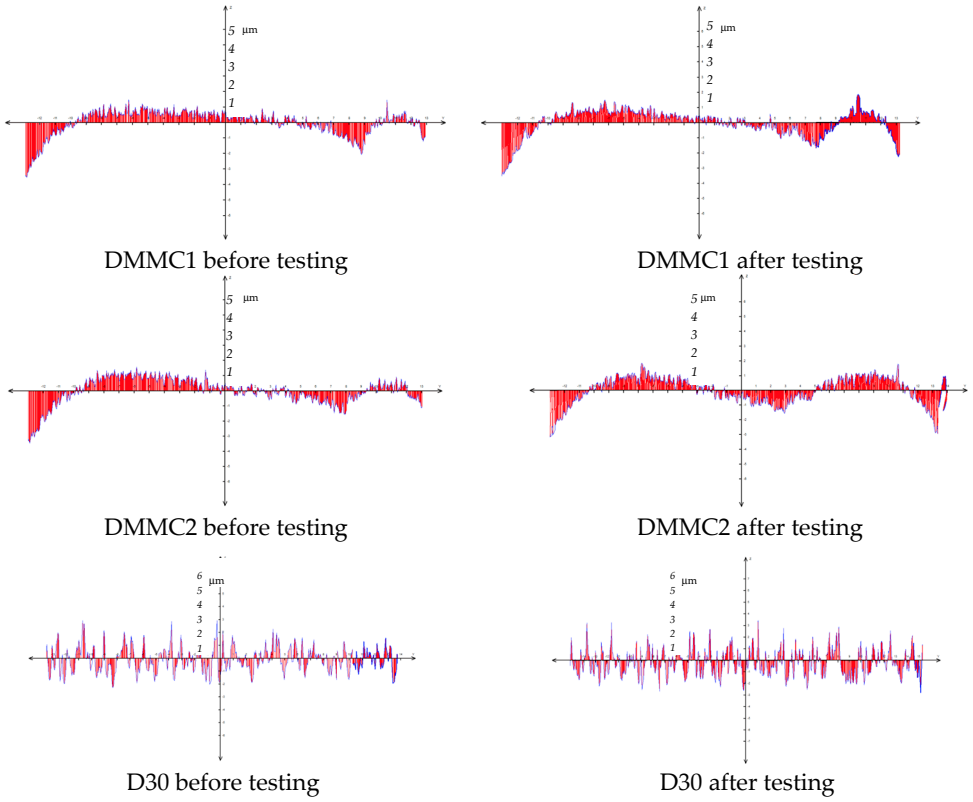

Figure 10. Diametral profile scan of disks before (**left**) and after (**right**) test (Y diameter direction).

When considering the entire set of experimental data obtained from tests carried out with the DMMC, it can be observed that volume losses were found to increase while values of the local linear speed decreased. In particular, this can be assessed by progressively considering the results of Test 1 and Test 2, carried out by using the same DMMC Specimen 1 (with linear speeds of 29.3 and 23.0 mm/s, respectively), and Test 3, run with the second coated disk DMMC Specimen 2 and with a linear speed of 14.7 mm/s. Results obtained for Test 4 (with the highest linear speed, equal to 34.5 mm) seem to deviate from the identified trend, with a volume loss that was found to be higher than expected. However, this can be explained by considering the higher surface roughness of the DMMC Specimen 2 (see Table 8), which, as proven by experimental observation, can counterbalance the effects of increasing contact speeds.

Results obtained from tests carried out with the D30 coating (Tests 5 and 6) suggest that when using a coarser material characterized by a rougher surface (see Table 8), higher

levels of abrasion are produced by making use of higher local linear speeds. It can also be observed that the use of the D30 coating leads to higher levels of wear (i.e., higher volume loss values) in comparison to those of DMMC coatings, with the consequent creation of a rougher final surface (see Table 7).

For D30 and DMMC Specimen 2, higher linear local speed results seem to be related to a higher abraded volume for both coatings. The same result can be found in the coating abrasion testing in [54], where this trend is justified by different abrasion phenomena occurring with increasing speed. Another piece of evidence is that the surface roughness of the disk is more influenced by abrasion than linear local speed. This piece of evidence will be better investigated when discussing the wear coefficient k and wear rate u.

Lastly, the effect of disk abrasion on ball average roughness values (R_a, R_q, Table 7) seems to not be affected by processing speed (Test 1 vs. Test 2; Test 3 vs. Test 4; Test 5 vs. Test 6) while it seems to be affected by abrading disk roughness (Test 1–4 vs. Test 5–6). On the other hand, the maximum roughness values (R_{vmax}, R_{pmax}, R_{zmax}, Table 7) seem to be affected by both abrasion speed (Test 1 vs. Test2; Test 3 vs. Test 4; Test 5 vs. Test 6) and by abrading disk roughness (Test 1–4 vs. Test 5–6).

In [21], the relationship between grain size and wear rate is discussed for diamond reinforced coatings against mild steel. In particular, it is reported that the wear rate increases with abrasive size. The increment changes from marginal to significant when the abrasive size is increased from 90 mm to 120 mm. The observation of the groove width and depth confirms this result. In the present research, the hardness of the surface subjected to abrasive wear, that is, Si_3N_4, is higher than mild steel, and the abrasion mechanism is different from [21] as a less ductile and more brittle material is interacting with diamond particles. Moreover, the influence of grain size is supposed to be less effective, as it can be observed in Figure 11, where the wear scars on the balls appear to be similar. Nevertheless, the ball roughness measurements reported in Table 7 show an agreement with [21]: a larger abrasive grain size (D30) generates a higher roughness and a larger wear rate. This effect is much more evident when comparing the trend of wear rate with grain size: it is evident that D30's higher abrasive grains are related to the higher wear rate of smaller grains size of DMMC.

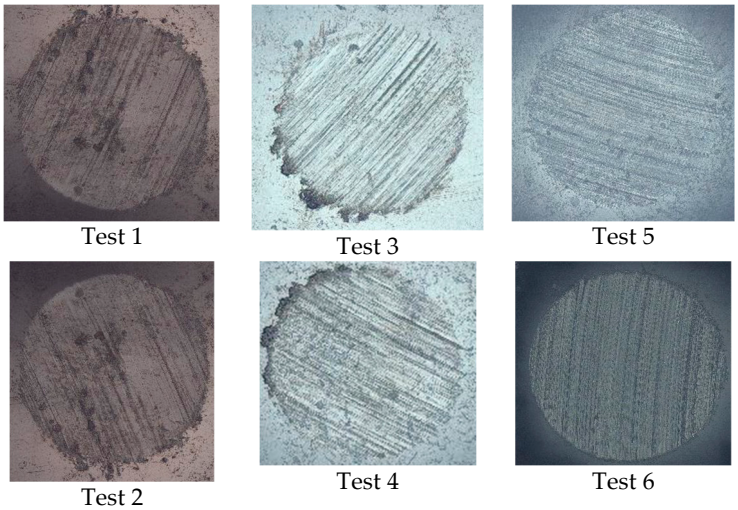

Figure 11. Wear scars on balls after testing.

The investigation of the abrasion mechanism of Si_3N_4 is widely reported in [58], where different Si_3N_4 microstructures were investigated. In the paper, a model of volume wear loss for brittle materials is discussed. For Si_3N_4, wear involves plastic deformation, which can be observed in the form of scars and wear sheet formation. The debris are compact, and they are mainly generated as wear sheet formed where the surface of silicon nitride is heavily deformed, that is at the edges of grooves. The same kind of abrasion of wear scars

is observed using a microscope in the Si_3N_4 balls tested in the present research (Figure 12). In [58], it is also reported that the principal mechanism of material abrasion for brittle materials is a subsurface fracture, which occurs mainly at microstructural heterogeneities, and generally is limited. The wear is mainly related to many factors such as contact surface, stress, speed, temperature, lubrication, and environment. In the discussed model, the properties of the abrading surface are not described. The abrasive behavior is related primarily to the hardness of the surface subjected to abrasive wear, the presence of protruded hard particles, and the capability of the hard particles to bear applied load so that it remained intact on the surface. In [58], the authors conclude that the low wear rate resulting from the investigated Si_3N_4 specimens does not assume that the wear model is reliable for Si_3N_4 brittle material.

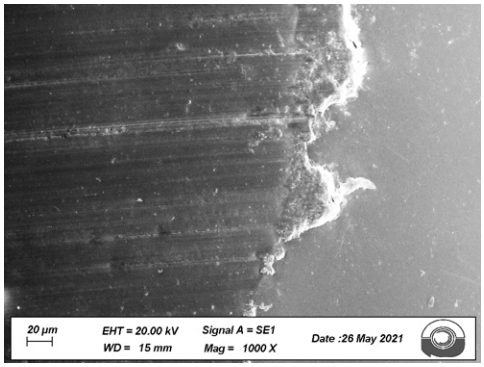

Figure 12. Detail of the edge of wear scar on ball after testing (Test 4).

From the analysis of Δ_{volume}, that is column 4 in Tables 9 and 10, the two different volume loss estimations, proposed in the two Standards [34,44], gave results with a difference lower than 8%. As reported, this difference does not affect the discussion of the results, and both formulations can be applied to compare the wearing performance of the two investigated coatings. Then, through the values of volume lost by the balls according to ASTM G99, the wear coefficient k and wear rate u (µm/h) of the six tests were calculated using Archard equation Equations (9) and (10). In Tables 11 and 12, the estimated values at R_t = 7 mm and 11 mm, respectively, are reported. Figures 13 and 14 show the wear coefficient and wear rates in µm/hour of the Si_3N_4 balls used during the six tests. In Table 12, the wear rate u (µm/h) related to Test 4 shows an abnormal value. The SEM observation of the wear track on the disk corresponding to this test showed that the copper coating of the disk was removed during the test, thus causing a rougher abrasive action of the diamond with respect to the other tests. According to [22], the wear rate is primarily governed by the protruding diamond particles on the coating surface. Then the higher abrasion performance of the D30 disk can be related to the higher surface roughness of D30 disks and, in particular, to the parameters R_{zmax}, which measures the maximum distance between peak and valleys, and R_{pmax}, which measures the maximum peak distance from the mean line.

Table 11. Wear coefficient k and wear rate u of Si_3N_4 ball for R_t = 7 mm.

	Wear Coefficient k (-)	**Wear Rate u (µm/h)**
Test 1	4.70×10^{-5}	5.21
Test 3	2.11×10^{-4}	5.32
Test 5	5.63×10^{-3}	27.58

Table 12. Wear coefficient k and wear rate u of Si_3N_4 ball for R_t = 11 mm.

	Wear Coefficient k (-)	Wear Rate u (µm/h)
Test 2	1.67×10^{-4}	7.43
Test 4	5.51×10^{-4}	20.28
Test 6	1.12×10^{-2}	91.68

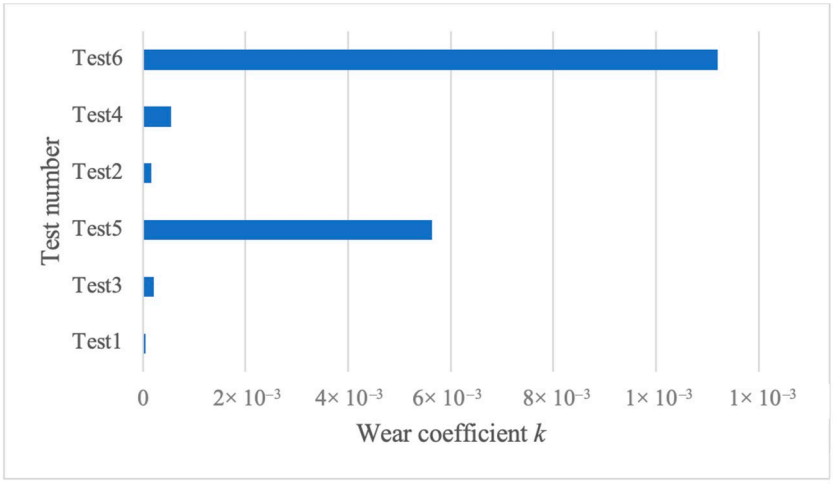

Figure 13. Wear coefficient k of Si_3N_4 balls.

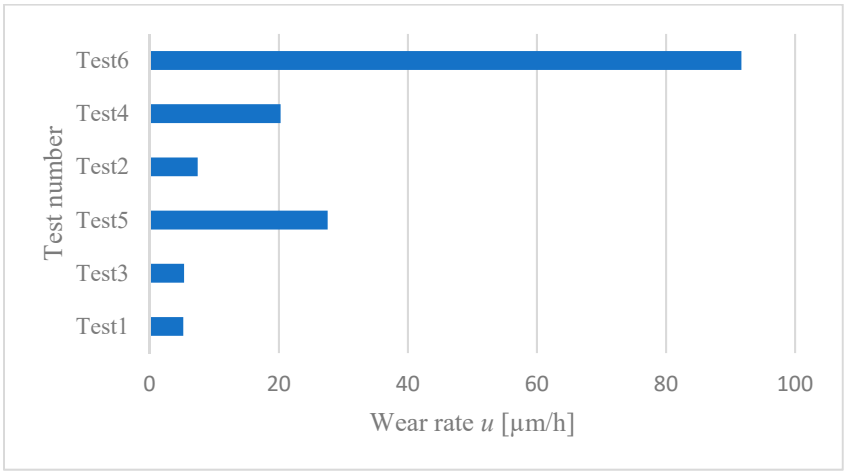

Figure 14. Wear rate u of Si_3N_4 balls.

It is evident that the D30 coating, which has a higher surface roughness value than the DMMC, performs a stronger abrasive action on the balls. In Figure 13, it can be observed that the wear coefficient k increases with increasing sliding linear speed (Test 5 vs. Test 6, Test 3 vs. Test 4). In fact, according to the model, in Equation (9), all the parameters are constant for the different testing conditions, and the variable is the abraded volume V_b, which increases with increasing local linear speed.

For what concerns the value of the friction coefficient COF, Table 13 reports the maximum value of the coefficient of friction COF for each test. The COF trends during the test are reported in Figure 15 for both DMMC and D30 samples.

Table 13. COF.

	Coefficient of Friction COF
Test 1	0.849
Test 2	0.816
Test 3	0.864
Test 4	0.874
Test 5	0.739
Test 6	0.832

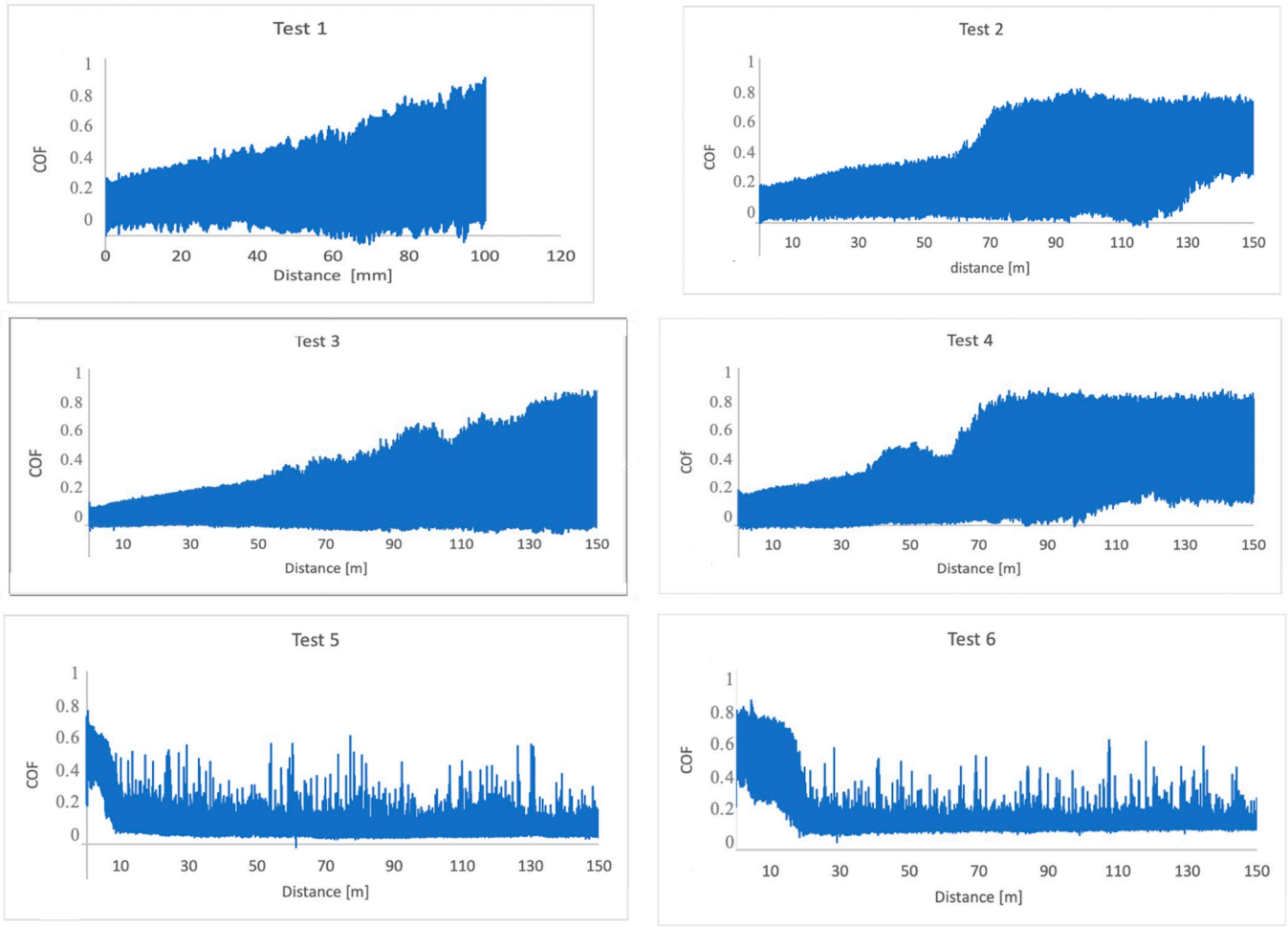

Figure 15. Trend of COF during test for DMMC (**first and second row**) and D30 (**third row**).

The observation of the COF related to Test 1 to Test 4, that is, the test run on the same coating (DMMC), shows similar values and trends, despite the small differences in surface roughness between the samples DMMC1 and DMMC2. For what concerns the D30 tests (Test 5 and Test 6), the COF shows a higher difference (about 20%).

In Figure 15, seemingly, the value of COF increases during the wear test for the DMMC sample; this is probably caused by the increase in the abraded surface of the ball in contact with the disk. This trend can be explained by considering the operating principle of the tribometer equipment. The COF is obtained as the ratio Ft/Fn, where Fn, the load applied during testing, is constant, and it is obtained by means of a weight positioned on a support; while Ft is obtained by measuring the power required to keep the rotating speed of the disk constant in the electric motor. When the contact surface increases, the Ft increases (and then the power required by the electric motor), and this is converted in an apparent increment in the COF, which is not actually occurring. Therefore, the greater the contact area, the

greater the value of the friction force with the same applied load, being the actual COF constant. This means that the COF estimated by the equipment is related to the contact surface, that is, to the *h* value and then to the wear rate. Then the COF apparently stabilizes. This stabilization occurs because the rate of increment of the contact surface decreases when the distance is decreased from the center of the ball, that is, with wear progressing. The contribution of variation of the wear rate due to the change in contact surface cannot be split from other contributions. Another cause of the apparent stabilization of the COF can be due to a sort of "saturation" of the disk with the debris of the ball, which acts as a sort of lubricant in friction and reduces the abrasive power of the disk.

In [59], the stabilization of the COF plot vs. the test length is discussed in terms of the relationship between friction and wear. This relationship is dependent on the fracture mechanism and the corresponding energy required to crack and generate debrides. This relationship can change over time with wear evolution due to temperature and other material property modifications. All these effects affect the trend of COF, and the estimation of their individual contribution requires a dedicated investigation.

The D30 sample COF plot shows an opposite trend. The sample has an elevated abrasive capacity and a relatively elevated COF, but soon the debrides of the Si_3N_4 ball deposit on the disk. This phenomenon involves a lubricant effect which causes the COF to drop down to a lower value. An in-depth analysis showed that, after the first few revolutions, the ball lost 70% of its material, which deposited on the disk, decreasing the abrasive capability of the disk and rendering it less effective. A similar effect is reported in [35], where during the in-pin on disk tests, in dry condition, the wear debris accumulated in the wear tracks; however, in lubrication condition wear debris accumulation was less. In [23], the COF obtained in the tests is two orders of magnitude lower than the above-mentioned results. This can be due to the different matrix in the coated disk composition, that is, Nickel.

In the present research, EDS analysis of the surfaces of the disks did not point out any noticeable difference in the two samples. In the present research the wear track was analysed in all the specimens, as reported in [21]. In all the samples, in the wear tracks, the presence of Si was relevant. In the DMMC specimen Al and O and in D30 specimen Fe traces were found, thus indicating that abrasion debrides deposited in the wear track and a probable abrasion of the coating can take place.

4. Conclusions

In the present research, an experimental analysis is reported comparing the abrasive behavior of two diamond coatings, DMMC and D30, against Si_3N_4 balls. The analysis was run by comparing the results of pin on disk tests in dry conditions considering the influence of different sliding speeds. Two Standards were applied to quantify the abrasive performance of the two coatings, the ASTM G99 and the ISO 18535. In particular, the abraded volume of Si_3N_4 balls was measured, and this value was selected as the base datum to calculate abrasion and friction parameters and to compare the abrasive performance of the two coatings.

The two coatings differ in deposition processes. These processes cause a different density of diamond particles, a different average and scatter of the dimension of the abrasive particle, and a different disk surface roughness.

The results pointed out that the parameters affecting the abrasion effectiveness of the coatings are the surface roughness and the sliding speed: increasing the sliding speed increases the abraded volume for both the coatings. Furthermore, it was found that a small increment in the abrasive particle size generated different surface roughness parameter values and a dramatic increment in the wear rate of the Si_3N_4 balls.

The D30 coating is more effective in abrasion than the DMMC coating. On the other hand, the surface finish of the balls processed with the DMMC coating is finer than the D30. From a technological point of view, the obtained results indicate that the two coatings may be employed in different phases of the manufacturing process.

Author Contributions: Conceptualization, R.S.; I.P.F.; validation, M.D.B.; formal analysis, R.L.; investigation, M.D.B.; writing—original draft preparation I.P.F., and R.S.; writing—review and editing, I.P.F.; R.S.; supervision, R.L. All authors have read and agreed to the published version of the manuscript.

Funding: This research received no external funding.

Data Availability Statement: Data are available on demand.

Conflicts of Interest: The authors declare no conflict of interest.

Nomenclature

l	Profilometer measured length
L	Sliding distance
n	Angular rotation speed
ν_c	Coating Poisson ratio
R_d	Disc radius
R_t	Track radius
v	Linear sliding speed
V_b	Volume ball loss
V_{bASTM}, V_{bISO}	Volume ball loss according to [34], to [47]
V_d	Volume disk loss
V_{dASTM}, V_{dISO}	Volume disk loss according to [34], to [47]
W_{sb}	Specific ball wear rate
W_{sd}	Specific disk wear rate

References

1. Liu, X.-J.; Huang, Z.-Y.; Ge, Q.-M.; Sun, X.-W.; Huang, L.-P. Microstructure and Mechanical Properties of Silicon Nitride Ceramics Prepared by Pressureless Sintering with MgO–Al_2O_3–SiO_2 as Sintering Additive. *J. Eur. Ceram. Soc.* **2005**, *25*, 3353–3359. [CrossRef]
2. Shi, Y.; Neubrand, A.; Koch, D. Characterization of Hardness and Stiffness of Ceramic Matrix Composites through Instrumented Indentation. *Test. Adv. Eng. Mater.* **2019**, *21*, 1800806. [CrossRef]
3. Herrmann, M.; Schuber, C.; Rendtel, A.; Hübner, H. Silicon Nitride/Silicon Carbide Nanocomposite Materials: I, Fabrication and Mechanical Properties at Room Temperature. *J. Am. Ceram. Soc.* **2005**, *81*, 1095–1108. [CrossRef]
4. Śmiga, W.; Garbarz-Glos, B. Structural and Mechanical Properties of Ceramic Solid Solutions $Na_{1-x}Li_xNbO_3$ for $x \leq 0.06$. *Ferroelectrics* **2008**, *377*, 137–145. [CrossRef]
5. Katz, R.N. Ceramic material for rolling element bearing applications. In *Friction and Wear of Ceramics*; Army Research Laboratory: Watertown, MA, USA, 1995; pp. 312–328.
6. Oliver, J.; Guerrero, G.; Goldman, J. Ceramic Bearings for Electric Motors. In Proceedings of the 2015 IEEE-IAS/PCA Cement Industry Conference, Toronto, ON, Canada, 26–30 April 2015.
7. Pakhomova, S.A.; Povalyayev, A.I. Silicon Nitride-Based Ceramic Composite Materials for Corrosion-Resistant Rolling Bearings. *IOP Conf. Ser. Mater. Sci. Eng.* **2019**, *683*, 012040. [CrossRef]
8. Wang, L.; Snidle, R.; Gu, L. Rolling Contact Silicon Nitride Bearing Technology: A Review of Recent Research. *Wear* **2000**, *246*, 159–173. [CrossRef]
9. Chen, S.; Liu, X.; Wan, L.; Gao, P.; Zhang, W.; Hou, Z. Effect of V2O5 Addition on the Wettability of Vitrified Bond to Diamond Abrasive and Grinding Performance of Diamond Wheels. *Diam. Relat. Mater.* **2020**, *102*, 107672. [CrossRef]
10. Pyun, H.-J.; Purushothaman, M.; Cho, B.-J.; Lee, J.-H.; Park, J.-G. Fabrication of High Performance Copper-Resin Lapping Plate for Sapphire: A Combined 2-Body and 3-Body Diamond Abrasive Wear on Sapphire. *Tribol. Int.* **2018**, *120*, 203–209. [CrossRef]
11. Sokolov, E.G.; Artem'ev, V.P.; Voronova, M.I. Study of the Structure and Hardness of Alloys of the Sn–Cu–Co System Used as Diamond Abrasive Tool Binders. *Met. Sci. Heat Treat.* **2017**, *59*, 321–324. [CrossRef]
12. Kubota, A.; Nagae, S.; Motoyama, S. High-Precision Mechanical Polishing Method for Diamond Substrate Using Micron-Sized Diamond Abrasive Grains. *Diam. Relat. Mater.* **2020**, *101*, 107644. [CrossRef]
13. The British Standards Institution. *BS ISO 6106: 2013 BSI Standards Publication Abrasive Products—Checking the Grain Size of Superabrasives*; The British Standards Institution: London, UK, 2013; pp. 1–18.
14. Baptista, A.; Silva, F.; Porteiro, J.; Miguez, J.; Pinto, G. Sputtering Physical Vapour Deposition (PVD) Coatings: A Critical Review on Process Improvement andMarket Trend Demands. *Coatings* **2018**, *8*, 402. [CrossRef]
15. Dezfuli, S.M.; Sabzi, M. Deposition of ceramic nanocomposite coatings by electroplating process: A review of layer-deposition mechanisms and effective parameters on the formation of the coating. *Ceram. Int.* **2019**, *45*, 21835–21842. [CrossRef]
16. Nasirpouri, F.; Alipour, K.; Daneshvar, F.; Sanaeian, M. Electrodeposition of Anticorrosion Nanocoatings. In *Corrosion Protection at the Nanoscale*; Elsevier: Amsterdam, The Netherlands, 2020; pp. 473–497.

17. Holmberg, K.; Matthews, A.; Ronkainen, H. Coatings Tribology—Contact Mechanisms and Surface Design. *Tribol. Int.* **1998**, *31*, 107–120. [CrossRef]
18. Yin, S.; Xie, Y.; Cizek, J.; Ekoi, E.J.; Hussain, T.; Dowling, D.P.; Lupoi, R. Advanced Diamond-Reinforced Metal Matrix Composites via Cold Spray: Properties and Deposition Mechanism. *Compos. Part B Eng.* **2017**, *113*, 44–54. [CrossRef]
19. Sharp, W.F. properties and applications of composite diamond coatings. *Wear* **1975**, *32*, 315–325. [CrossRef]
20. Richardson, A.; Neville, A.; Wilson, J.I. Developing Diamond MMCs to Improve Durability in Aggressive Abrasive Conditions. *Wear* **2003**, *255*, 593–605. [CrossRef]
21. Venkateswarlu, K.; Ray, A.K.; Gunjan, M.K.; Mondal, D.P.; Pathak, L.C. Tribological Wear Behavior of Diamond Reinforced Composite Coating. *Mater. Sci. Eng. A* **2006**, *418*, 357–363. [CrossRef]
22. Venkateswarlu, K.; Rajinikanth, V.; Naveen, T.; Sinha, D.P.; Atiquzzaman Ray, A.K. Abrasive Wear Behavior of Thermally Sprayed Diamond Reinforced Composite Coating Deposited with Both Oxy-Acetylene and HVOF Techniques. *Wear* **2009**, *266*, 995–1002. [CrossRef]
23. Yang, L.; Li, B.; Yao, J.; Li, Z. Effects of Diamond Size on the Deposition Characteristic and Tribological Behavior of Diamond/Ni60 Composite Coating Prepared by Supersonic Laser Deposition. *Diam. Relat. Mater.* **2015**, *58*, 139–148. [CrossRef]
24. Qin, F.; Chou, Y.K.; Nolen, D.; Thompson, R.G. Coating Thickness Effects on Diamond Coated Cutting Tools. *Surf. Coatings Technol.* **2009**, *204*, 1056–1060. [CrossRef]
25. Chu, K.; Liu, Z.; Jia, C.; Chen, H.; Liang, X.; Gao, W.; Tian, W.; Guo, H. Thermal Conductivity of SPS Consolidated Cu/Diamond Composites with Cr-Coated Diamond Particles. *J. Alloys Compd.* **2010**, *490*, 453–458. [CrossRef]
26. Abyzov, A.M.; Kidalov, S.V.; Shakhov, F.M. High Thermal Conductivity Composite of Diamond Particles with Tungsten Coating in a Copper Matrix for Heat Sink Application. *Appl. Therm. Eng.* **2012**, *48*, 72–80. [CrossRef]
27. Abdullah, M.Z.; Abdullah, A.N.; bin Othman, M.H.; Ahmad, M.A.; Hussain, P. Pin-on-disc tribotest of Cr/CrN/CrCN/ZrN multilayer coatings by physical vapour deposition (PVD). *Mater. Today: Proc.* **2019**, *16*, 2067–2071.
28. Umehara, N.; Kirtane, T.; Gerlick, R.; Jain, V.K.; Komanduri, R. A New Apparatus for Finishing Large Size/Large Batch Silicon Nitride (Si3N4) Balls for Hybrid Bearing Applications by Magnetic Float Polishing (MFP). *Int. J. Mach. Tools Manuf.* **2006**, *46*, 151–169. [CrossRef]
29. *ASTM G65—Standard Test Method for Measuring Abrasion Using the Dry Sand/Rubber Wheel Apparatus*; ASTM International: West Conshohocken, PA, USA, 2016; Volume 5, pp. 1–14.
30. Gates, J.D. Two-body and three-body abrasion: A critical discussion. *Wear* **1998**, *214*, 139–146. [CrossRef]
31. Suzukib, K.; Sato, K.; Yokoyama, T. Production of Electrodeposited Diamond Wheels and Grinding Performance for Hard Metals and Ceramics. *J. Mater. Process. Technol.* **1996**, *62*, 303–308.
32. Dosta, S.; Couto, M.; Guilemany, J.M. Cold Spray Deposition of a WC-25Co Cermet onto Al7075-T6 and Carbon Steel Substrates. *Acta Mater.* **2013**, *61*, 643–652. [CrossRef]
33. Salguero, J.; Vazquez-Martinez, J.; Sol, I.; Batista, M. Application of Pin-On-Disc Techniques for the Study of Tribological Interferences in the Dry Machining of A92024-T3 (Al–Cu) Alloys. *Materials* **2018**, *11*, 1236. [CrossRef]
34. ASTM G99. *G99, Standard Test Method for Wear Testing with a Pin-on-Disk Apparatus*; ASTM International: West Conshohocken, PA, USA, 2006; Volume 5, pp. 1–6.
35. ASTM G133. *Standard Test Method for Linearly Reciprocating Ball-on-Flat Sliding Wear 1*; ASTM International: West Conshohocken, PA, USA, 2011; Volume 5, pp. 1–10.
36. ISO 4287:1997. Geometrical Product Specifications (GPS)—Surface Texture: Profile Method—Terms, Definitions and Surface Texture Parameters. *Int. Organ. Stand.* **1997**, 1–38.
37. Rizzo, A.; Giannuzzi, M.; Massaro, M.; Dimaio, D.; Papadia, G. Validation of TiAlN functional coatings through cryo-tribological characterization using a pin on disk experiment. *Procedia CIRP* **2021**, *99*, 295–300. [CrossRef]
38. Goti, E.; Mazza, L.; Mura, A.; Zhang, B. An early method for the technical diagnosis of pin-on-disk tribometers by reference friction measurements in EHL conditions. *Measurement* **2020**, *166*, 108169. [CrossRef]
39. Jana, A.; Dandapat, N.; Das, M.; Balla, V.K.; Chakraborty, S.; Saha, R.; Mallik, A.K. Severe Wear Behaviour of Alumina Balls Sliding against Diamond Ceramic Coatings. *Bull. Mater. Sci.* **2016**, *39*, 573–586. [CrossRef]
40. Qin, W.; Yue, W.; Wang, C. Controllable Wear Behaviors of Silicon Nitride Sliding against Sintered Polycrystalline Diamond via Altering Humidity. *J. Am. Ceram. Soc.* **2018**, *101*, 2506–2515. [CrossRef]
41. Yue, T.; Yue, W.; Qin, W.; Liu, P.; Wang, C. Effects of Environmental Atmospheres on Tribological Behaviors of Sintered Polycrystalline Diamond Sliding against Silicon Nitride. *Int. J. Refract. Met. Hard Mater.* **2019**, *81*, 85–93. [CrossRef]
42. Qin, W.; Liu, Y.; Yue, W.; Wang, C.; Ma, G.; Wang, H. Influence of Frictional Interface State on Tribological Performance of Sintered Polycrystalline Diamond Sliding Against Different Mating Materials. *Tribol. Lett.* **2019**, *67*, 87. [CrossRef]
43. Li, J.; Yue, W.; Qin, W.; Wang, C. Approach to Controllable Tribological Properties of Sintered Polycrystalline Diamond Compact through Annealing Treatment. *Carbon N. Y.* **2017**, *116*, 103–112. [CrossRef]
44. Sha, X.; Feng, B.; Yue, W.; Wang, C. Grain Size Dependent Tribological Behaviors of 700 °C Annealed Polycrystalline Diamond. *Int. J. Refract. Met. Hard Mater.* **2021**, *94*, 105406. [CrossRef]
45. Li, J.; Yue, W.; Qin, W.; Mao, Q.; Gao, B.; Li, Y. Effect of Quenching Processes on Microstructures and Tribological Behaviors of Polycrystalline Diamond Compact (PCD/WC-Co) in Annealing Treatment. *Diam. Relat. Mater.* **2017**, *79*, 79–87. [CrossRef]

46. Li, Y.; Sha, X.; Yue, W.; Qin, W.; Wang, C. Effects of Tribochemical Reaction on Tribological Behaviors of Si3N4/Polycrystalline Diamond in Hydrochloric Acid. *Int. J. Refract. Met. Hard Mater.* **2019**, *79*, 197–203. [CrossRef]
47. International Organization for Standardization. *International Standard ISO 18535:2016—Diamond-like Carbon Films—Determination of Friction and Wear Characteristics of Diamond-Like Carbon Films by Ball-on-Disc Method*; International Organization for Standardization: Geneva, Switzerland, 2012; pp. 1–24.
48. Tian, X.; Qiao, H.; Chu, X. Wear Performance of Bonded Composite Coatings under Dry Sliding. *Surf. Coatings Technol.* **2014**, *240*, 191–196. [CrossRef]
49. Archard, J.F. Contact and Rubbing of Flat Surfaces. *J. Appl. Phys.* **1953**, *24*, 981–988. [CrossRef]
50. Kontou, A.; Southby, M.; Spikes, H.A. Effect of Steel Hardness on Soot Wear. *Wear* **2017**, *390–391*, 236–245. [CrossRef]
51. Liu, Y.; Liskiewicz, T.W.; Beake, B.D. Dynamic Changes of Mechanical Properties Induced by Friction in the Archard Wear Model. *Wear* **2019**, *428–429*, 366–375. [CrossRef]
52. Miranda, J.C.; Ramalho, A. Study of the Effects of Damage Accumulation on Wear. *Wear* **2015**, *330–331*, 79–84. [CrossRef]
53. Tunalioğlu, M.Ş.; Tuç, B. Theoretical and Experimental Investigation of Wear in Internal Gears. *Wear* **2014**, *309*, 208–215. [CrossRef]
54. Hogmark, S.; Jacobson, S.; Larsson, M. Design and Evaluation of Tribological Coatings. *Wear* **2000**, *246*, 20–33. [CrossRef]
55. Sala, G.; Landro, L.; Di Airoldi, A.; Bettini, P. *Tecniche e Tecnologie dei Materiali Aerospaziali*; 1941; pp. 1–17. (In Italian)
56. Kottfer, D.; Ferdinandy, M.; Kaczmarek, L.; Maňková, I.; Beňo, J. Investigation of Ti and Cr Based PVD Coatings Deposited onto HSS Co 5 Twist Drills. *Appl. Surf. Sci.* **2013**, *282*, 770–776. [CrossRef]
57. Colbert, R.S.; Krick, B.A.; Dunn, A.C.; Vail, J.R.; Argibay, N.; Sawyer, W.G. Uncertainty in Pin-on-Disk Wear Volume Measurements Using Surface Scanning Techniques. *Tribol. Lett.* **2011**, *42*, 129–131. [CrossRef]
58. Dogan, C.P.; Hawk, J.A. Microstructure and abrasive wear in silicon nitride ceramics. *Wear* **2001**, *250*, 256–263. [CrossRef]
59. Blau, P.J. The significance and use of the friction coefficient. *Tribol. Int.* **2001**, *34*, 585–591. [CrossRef]